J. Phys. D: Appl. Phys. **44** (2011) 000000 (9pp) UNCORRECTED PROOF

Influence of SiC reinforcement particles on the tribocorrosion behaviour of Al–SiC_p FGMs in 0.05M NaCl solution

A C Vieira[1], L A Rocha[1] and S Mischler[2]

[1] Centre for Mechanical and Materials Technologies (CT2M) and Department of Mechanical Engineering, University of Minho, Azurém, 4800-058 Guimarães, Portugal
[2] Ecole Polytechnique Fédérale de Lausanne (EPFL), Tribology and Interface Chemistry Group, 1015 Lausanne, Switzerland

E-mail: catarina.vieira@engmateriais.eng.uminho.pt (Ana Catarina Vieira)

Received 13 December 2010, in final form 7 March 2011
Published
Online at stacks.iop.org/JPhysD/44

Abstract
The main aim of this work was to study and understand the influence of SiC particles on the corrosion and tribocorrosion of Al-matrix composite materials. For that, Al–SiC_p functionally graded composites were produced by centrifugal casting and different SiC_p contents were achieved. Their mechanical properties were improved by age-hardening heat treatments. The tribocorrosion behaviour was studied in 0.05M NaCl solutions using a reciprocating motion tribometer involving an alumina ball sliding against the Al-based samples. Above critical SiC particles' content the matrix alloy surface was found protected against wear by SiC particles protruding from the surface. Below this threshold content, the SiC reinforcement was inefficient and the wear rate of the composite was the same as the non-reinforced alloy.

AQ1 (Some figures in this article are in colour only in the electronic version)

1. Introduction

A functionally graded material (FGM) can be defined as a material with two or more phases, which varies in some spatial direction its composition and/or microstructure. The concept of composite material may be used to design FGMs, taking benefit of an inhomogeneous distribution of the reinforcing phase (metallic, ceramic or polymeric) resulting in an improvement of mechanical, thermal, electromagnetic, biochemical or biomechanical properties [1, 2–7]. For instances, using centrifugal casting, SiC particles can be dispersed in an Al-based matrix with a graded distribution originating an Al–SiC_p FGM [8, 9]. Therefore, it is possible to combine surface hardness and high wear resistance with high bulk toughness [10].

In fact, Al–SiC_p FGMs have shown a great potential for several industries [10, 11], being their major applications in electronic packaging industry, brake rotor assemblies or pistons rings in automotive industries and turbine components or rocket nozzles (relatively high-temperature environments) for advanced aircrafts and aerospace vehicles [1, 12–15].

Because of the relatively good corrosion properties of aluminium, Al–SiC_p FGMs are candidate materials for tribocorrosion applications were contact is exposed to the combined degradation by wear and corrosion. Examples of such tribocorrosion applications are chemical pumps, piston rings, cylinder walls and components in marine structures [16–18]. However, relatively little is known about the corrosion and tribocorrosion behaviour of aluminium-based FGMs.

The reinforcement by SiC particles can influence the corrosion behaviour of the Al matrix. Preferential attack at the reinforcement/matrix interface (due to Al_4C_3 formation at the interface), creation of local cathodes on conductive SiC catalysing the reduction of oxygen and/or modifications of the matrix alloy microstructure (alteration of the size and distribution of intermetallic phases) during composite production were phenomena reported in the literature as having influence on the corrosion resistance of Al–SiC_p composites [16, 19, 20]. Clearly, these effects are highly dependent on the nature of the matrix Al alloy, on the SiC particles and on the heat treatments.

JNL: JPD PIPS: 378401 TYPE: PAP TS: NEWGEN DATE: 28/3/2011 EDITOR: MJ SPELLING: UK

Also, the tribocorrosion behaviour of the material appears to be determined by the area fraction of reinforcement, particle mean size and tribological testing parameters. Velhinho *et al* [11] investigated the tribocorrosion behaviour of Al–SiC_p functionally graded composites against cast iron pins in water using a unidirectional pin on disc tribometer. Two volume fractions (12.6 and 35.7%) of SiC particles with median size of 118 μm were considered. Those authors reported that the presence of water facilitated catastrophic SiC particle pull-out, and therefore significantly increased wear. Indeed, higher volume fractions of SiC particles were found to cause larger wear. On the other hand, Gomes *et al* [21] also studied Al–SiC_p functionally graded composites but using different experimental conditions: reciprocating sliding and a normal load of 10 N. Tests were conducted using cast iron pins' counterfaces in a 3% NaCl solution and SiC particles' area fraction varying between 25.8% and 33.4%. In this case, the wear rate of the composites was not significantly affected by the presence of the aqueous solution. In contrast to Velhinho *et al* [11] results, higher amounts of reinforcement lead to lower wear rates. This behaviour was attributed to the capability of the SiC particles to anchor protective tribolayers and to their load-supporting effect allowing the protection of the Al matrix, contributing to a lower total wear of the composite material.

Fang *et al* [16] studied the synergistic effects of wear and corrosion for Al_2O_3 particulate–reinforced 6061 Al-matrix composites and postulated that, although the incorporation of reinforcement was detrimental to the corrosion resistance of the material, its influence on wear corrosion was favourable. Therefore, there is still a need for a mechanistic understanding of the involved phenomena.

This study aim was to gain a better understanding of the tribocorrosion mechanisms of Al–SiC_p functionally graded composites. For this a model system consisting of Al–SiC_p samples sliding against inert alumina balls in 0.05M NaCl was investigated. Aluminium matrix composites' materials with a gradient in SiC content were fabricated using centrifugal casting. Samples of different SiC contents were obtained by machining the composite ingots in different locations. Heat treatments were carried out in order to improve the mechanical properties of the matrix. The corrosion mechanisms were evaluated using immersion and electrochemical techniques. During tribocorrosion the open circuit potential (OCP) was recorded in order to gain information on the prevailing mechanisms.

2. Experimental details

2.1. Materials

A non-commercial Al–10Si–4.5Cu–2Mg (wt%) was selected as matrix of the composite. The alloy was home-developed in order to present specific properties, such as good castability (by adding Si), heat-treatment capability (by adding Cu) and good wettability (by adding Mg). As reinforcement, SiC particles with 37.6 μm as grain size distribution (10% of volumetric fraction) were selected. The FGMs were processed by centrifugal casting, using radial geometry, with 1500 rpm centrifugal speed.

Two different post-processing age-hardening heat treatments were made: solution treatment at 500 °C (2 h and 8 h), followed by quenching, plus an artificial ageing at 160 °C for 512 min. The solution treatments were made in air, in tubular furnace, while the artificial ageing was made in a thermostatic silicone bath (Model Haake F6).

In this paper the sample solutions treated for 2 h were identified as FGM-S2h while the sample solutions treated for 8 h were identified as FGM-S8h. To use as reference, a non-heat-treated sample was also studied and was identified as FGM-NHT.

The FGM microstructure was characterized using XRD (Cu Kα radiation, continuous Bragg Brentano mode, scan step size of 0.02°, Bruker D8 Discover equipment), SEM/EDS (Nano-SEM FEI Nova 200) and optical microscopy.

The particle area fraction was estimated by image analysis. For that, 25 to 30 images were acquired in an optical microscope and subsequently analysed with computer aided image analysis (Image tool 3.0).

Macro Vickers hardness measurements (30 kg, 20 s dwell time) were performed on all samples.

2.2. Corrosion tests

The samples were machined from the centrifugal cast-ring, in order to test the most exterior zone of the ring. Previous to each corrosion test, the samples were wet-polished up to 1200 mesh in SiC abrasive paper.

The electrochemical solution used was 0.05M NaCl (pH = 6.2). The pH was measured before and after the corrosion tests. No variation in the pH was detected during the tests.

Two types of tests were carried out: immersion tests (to characterize localized corrosion mechanisms) and potentiodynamic polarization measurements (polarization curves). In the first tests, the samples were immersed in the solution (open circuit conditions) for 30 min and afterwards the corroded samples were analysed by SEM. Regarding the polarization curves, a potential sweep rate of 0.5 mV s^{-1} in the noble direction (starting from cathodic values) was used. The samples were stabilized in the solutions for 1 h before these measurements. A three-electrode electrochemical cell configuration integrating a standard double wall glass cell was used: a standard calomel reference electrode (SCE), a Pt counter electrode and the FGM samples connected as working electrode (WE) to the potentiostat (Autolab PGSTAT 30 under GPES software). In this paper, all potentials are given with respect to SCE.

2.3. Tribocorrosion tests

Discs were machined from the most exterior part of the centrifugal cast-ring, with $\varnothing$ = 20 mm (±0.1 mm) and 5 mm (±0.1) thick. Previous to each test, the samples were polished down to 3 μm diamond spray (from Struers). The surface roughness (R_a) was measured after polishing. R_a was of 0.21 ± 0.07 μm in the FGM samples. R_a values of the unreinforced centrifuged Al matrix was of 0.04 ± 0.01 μm.

The tribocorrosion experiments were performed using the solution described above. The pH was evaluated before and after tribocorrosion tests to verify that no changes occurred during rubbing. The tests were done at OCP conditions in a reciprocating ball-on-plate tribometer (ball sliding against a stationary WE), with 1 Hz frequency, 4 mm stroke length, 11.4 mm s^{-1} as sliding velocity and 4 N as normal applied load (at approximately 22 °C and relative humidity of 40%). The counterbody was an alumina ball ($\varnothing = 6$ mm). Details on the tribometer used in this study can be found elsewhere [22, 23].

An electrochemical cell was mounted on the tribometer with a three electrodes configuration. The FGM sample was connected to a Wenking LB 95 L potentiostat as WE. A Pt counter electrode and a SCE completed the electrochemical set-up.

The profiles of the wear tracks were quantified using non-contact scanning laser profilometry (UBM Telefokus instrument). Three profiles across the wear track for each sample were measured. The wear volume was calculated by multiplying the depth mean values by the track's length (4 mm) and by the width.

The worn surfaces were analysed by SEM/EDS. EDS spectra were obtained under an acceleration voltage of 15 KeV. The SEM/EDS equipment used were a Nano-SEM model—FEI Nova 200.

3. Results

3.1. Materials microstructural characterization

The FGM-NHT, FGM-S2h and FGM-S8h microstructural characterization was made by XRD and SEM, previous to corrosion and tribocorrosion tests. From the XRD pattern, presented in figure 1, FGM-NHT, FGM-S2h and FGM-S8h samples presented the same phases: α-Al, Si, θ (Al_2Cu), Q ($Al_4Cu_2Mg_8Si_7$), π ($Al_8Si_6Mg_3Fe$) and SiC. The first five phases were from the Al matrix [24], being SiC the reinforcement phase.

The microstructures of FGM-NHT, FGM-S2h and FGM-S8h are presented in figure 2. No significant differences can be observed between the samples, being the only dissimilarity related with the whitest phase identified by EDS as the Cu-rich phase θ-Al_2Cu [24]. In figure 2(*d*)) an EDS spectra obtained on the θ-Al_2Cu phases from the FGM-NHT sample are presented, confirming the presence of Al and Cu. Similar spectra were obtained in FGM-S2h and FGM-S8h samples. The heat treatment on the FGM samples leads to more fine and dispersed Cu-rich phases. From our previous work [24], the distribution and size of the Q-$Al_4Cu_2Mg_8Si_7$ and the π-$Al_8Si_6Mg_3Fe$ phases on Al-matrix alloys were shown to be not affected by the heat treatments. On the other hand, the θ-Al_2Cu and Si phases become more fine and dispersed after the heat treatment, being the decrease in size of the θ-Al_2Cu phase confirmed by image analysis.

Table 1 lists the SiC particle area fraction as determined by image analysis. The hardness values of each sample are also presented in table 1. Hardness increases with increasing SiC particle area fraction. This correlation was already reported in previous works [10, 25].

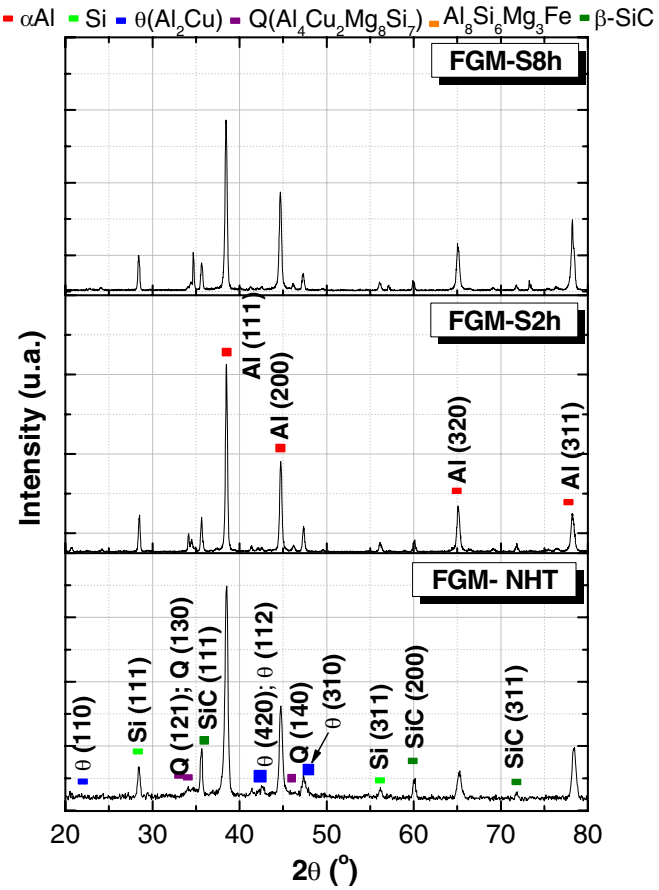

Figure 1. XRD patterns obtained in the Al–SiC_p FGM-NHT, FGM-S2h and FGM-S8h samples.

Regarding the hardness mean values presented in table 1, the lower hardness values were obtained in FGM-NHT (samples without heat treatment), while the highest values were obtained with the FGM-S2h and FGM-S8h heat-treated samples.

3.2. Corrosion behaviour

The surface morphology of FGM-NHT sample, after immersion tests, is presented in figure 3. There is preferential dissolution of the Al matrix around the θ-Al_2Cu phases (figure 3(*a*)), by the formation of a galvanic couple between the Cu-rich phases (preferential cathodes) and the surrounding Al matrix (preferential anodes). This mechanism was confirmed as the main corrosion mechanism presented in the Al alloy matrix [24]. From figure 3(*b*), no preferential attack at the reinforcement/matrix interface as well as preferential dissolution of Al matrix around the SiC reinforcement particle can be noticed. Therefore, no effect of SiC reinforcement particles on the corrosion mechanisms can be suggested. This shows that SiC reinforcement does not alter, in the present conditions, the corrosion mechanisms of these Al alloys. Similar behaviour was observed in FGM-S2h and FGM-S8h samples when immersed in NaCl solution.

Figure 4 presents the potentiodynamic polarization curves of the FGM samples in NaCl solution. For comparison,

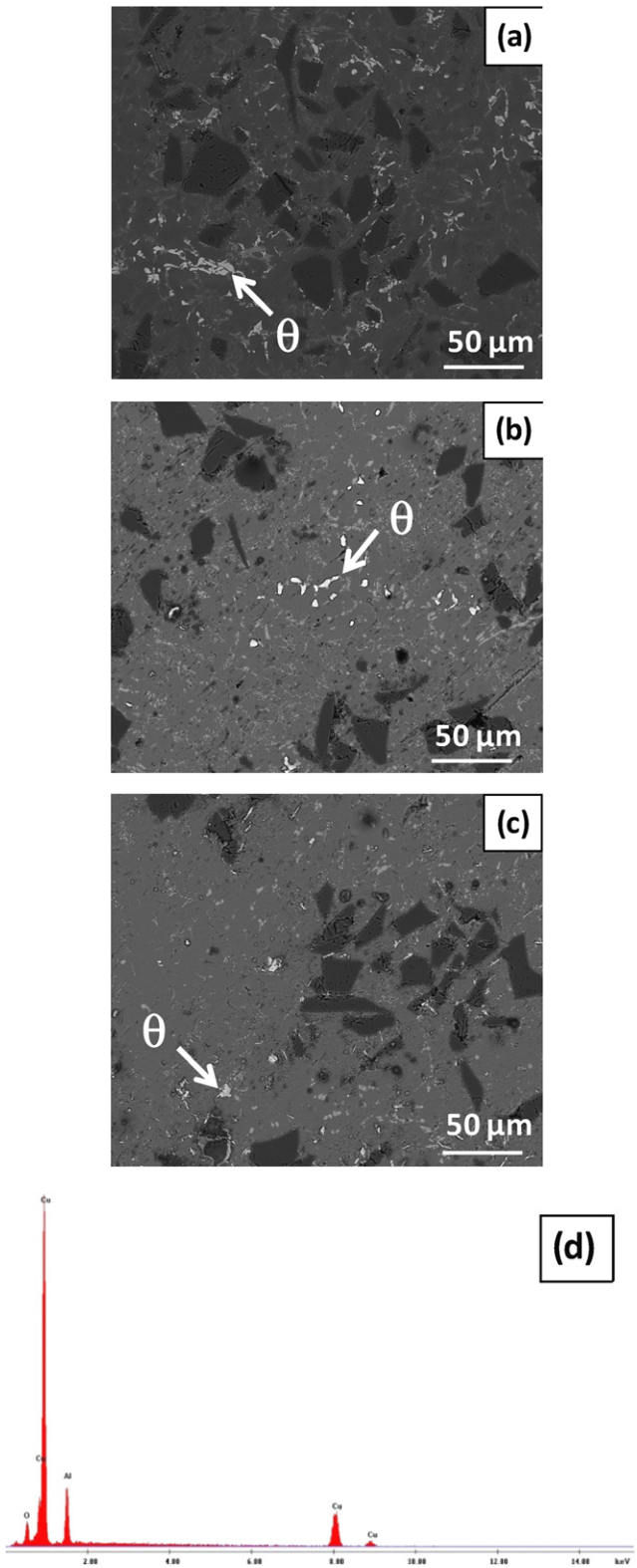

Figure 2. SEM micrographs obtained in backscattering electron mode (BE mode) of (*a*) FGM-NHT, (*b*) FGM-S2h, (*c*) FGM-S8h, (*d*) EDS spectra obtained on the θ phases presented in FGM-NHT sample.

the polarization curve obtained with unreinforced Al matrix (without SiC reinforcement particles) is also presented. The reproducibility of the tests being very good, only one curve per condition was plotted. No significant differences can

Table 1. Characterization of the samples tested in the tribocorrosion tests in 0.05M NaCl solution, regarding the SiC particle area fraction on the surface sample and macro Vickers hardness (HV_{30}).

	SiC particle area fraction (%)	HV_{30}	HV_{30} (mean values)
FGM-NHT	15 ± 3	135 ± 6	140 ± 18
	17 ± 5	141 ± 3	
	23 ± 4	159 ± 13	
FGM-S2h	14 ± 6	176 ± 4	179 ± 10
	16 ± 4	180 ± 6	
	18 ± 3	189 ± 11	
FGM-S8h	11 ± 3	180 ± 0	177 ± 9
	18 ± 3	181 ± 6	

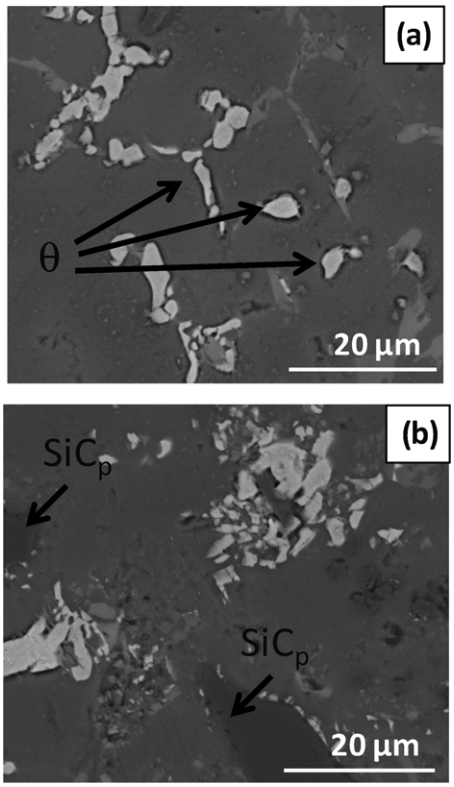

Figure 3. SEM micrographs obtained in FGM-NHT sample after immersion tests of 30 min in 0.05M NaCl solution (backscattering electron mode): (*a*) identification of θ-Al_2Cu phases; (*b*) identification of SiC particles. Similar micrographs were identified in FGM-S2h and in FGM-S8h samples.

be detected between the different samples. E_{corr} is similar to all the samples (≈ -0.60 V). Therefore, in NaCl solution, apparently, neither the presence of SiC particles nor the heat treatment does significantly influence the corrosion behaviour of the material.

3.3. Tribocorrosion behaviour

The evolution of the OCP with time during tribocorrosion testing of FGM-NHT, FGM-S2h and FGM-S8h samples of different SiC particle contents are presented in figures 5(*a*), (*b*) and (*c*), respectively. Each test was identified in accordance with the SiC particle area fraction value presented on the tested sample surface. For comparison, the results obtained with

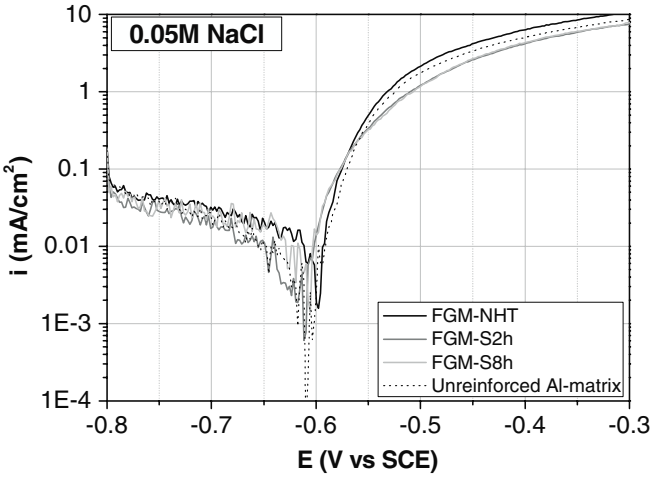

Figure 4. Polarization curves of FGM-NHT, FGM-S2h, FGM-S8h and unreinforced Al matrix samples in 0.05M NaCl solution.

unreinforced Al-matrix samples (without SiC_p and identified in the figures with 0%) are also presented. Before rubbing, the corrosion potential values are similar in all the samples (approximately −0.6 V). The OCP decreases when rubbing starts. This behaviour is usually attributed to the breaking of the passive film on the wear track area by the abrading alumina ball [17, 26–28]. Once rubbing stops depassivation ceases and the potential recovers its initial value.

During rubbing, between 1200s and 1800s, samples without SiC and samples with lower SiC particles' area fraction values have OCP values in the range −0.9 V to −1.0 V. This trend indicates that during rubbing, the material surface in being constantly depassivated. However, for higher SiC particles' area fraction values (for instances, 23 ± 4% in figure 5(*a*)), after the initial cathodic shift, the OCP recovers during rubbing reaching the value observed before sliding, suggesting that repassivation of the sample surface occurred during rubbing.

In the case of repassivation occurring during rubbing, a correlation between the evolution of OCP and friction coefficient with time was observed (figure 6(*a*)), where negative peaks in OCP correspond to positive peaks in friction coefficient. When repassivation did not occur during rubbing, the coefficient of friction attained more stable values within short time (figure 6(*b*)). This behaviour was observed systematically in heat-treated samples as well on the non-heat-treated material.

The wear volume estimated after the tribocorrosion samples are presented as a function of the SiC particles' area fraction in figure 7. For comparison data, the unreinforced alloys [22] are also plotted. The SiC reinforcement does not affect significantly wear volume values up to a volume fraction of approximately 15% above which a steady decrease in wear is observed. The minimum wear volume values were achieved to volume fraction similar or higher than 18%. The low wear volumes exhibited by FGM-S2h and FGM-S8h samples are likely due to the increase in hardness induced by the heat treatment.

Two typical wear patterns were observed using SEM. The first one corresponds to heat-treated and non-heat-treated

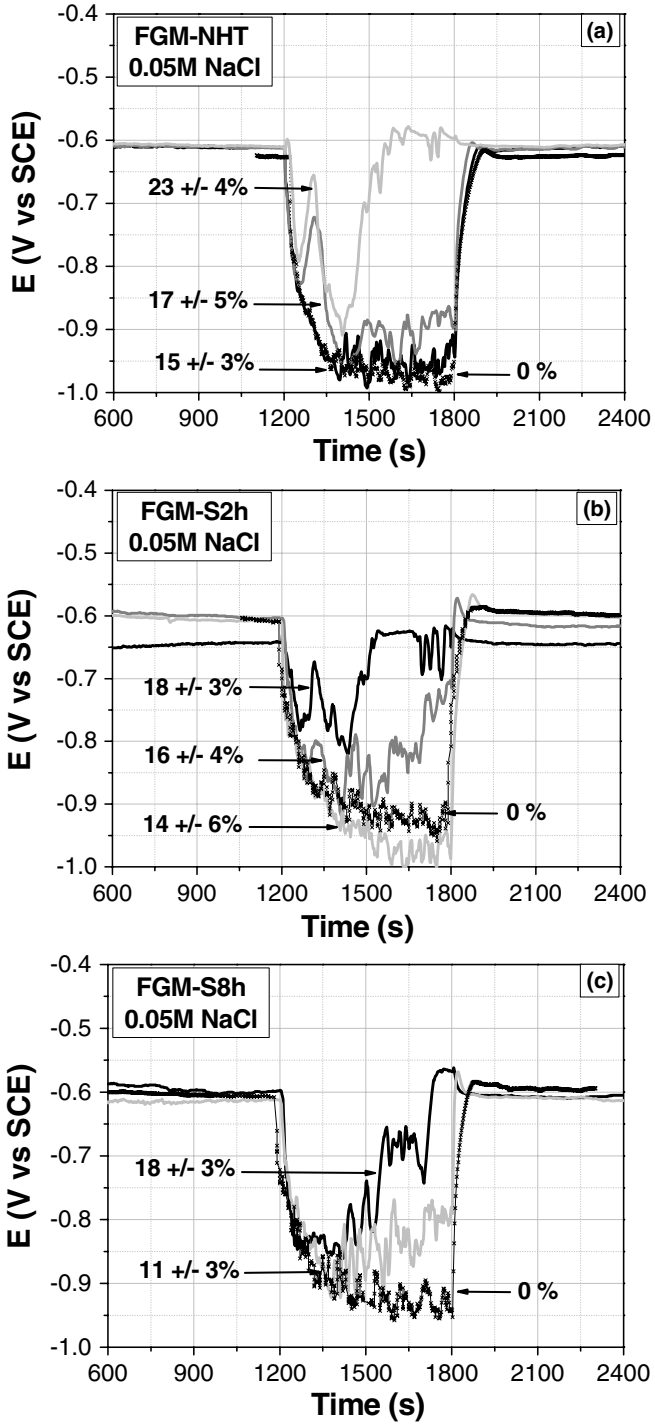

Figure 5. Corrosion potential evolution with time during the tribocorrosion tests in (*a*) FGM-NHT, (*b*) FGM-S2h, (*c*) FGM-S8h samples tested in 0.05M NaCl solution. Each test is identified in accordance with the SiC particle area fraction value presented on the sample surface.

samples with SiC contents lower or equal to 15% where large plastic flow and material smearing characterize the worn surface (figure 8(*a*)). The two large pits (approximately 30 μm) observed in figure 8(*a*) are likely due to the pull-out of SiC particles. The second characteristic pattern is observed on samples with SiC contents higher than 18%. These samples present a more corrugated topography with

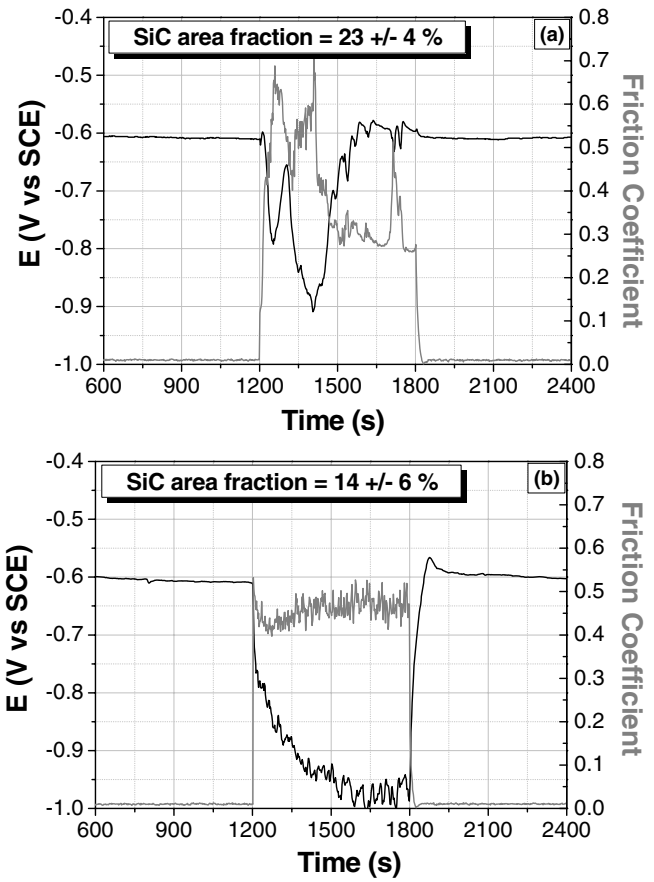

Figure 6. Friction coefficient and corrosion potential evolution during the tribocorrosion tests in 0.05M NaCl for (*a*) FGM-NHT with 23 ± 4% SiC, (*b*) FGM-S2h with 14 ± 6% SiC.

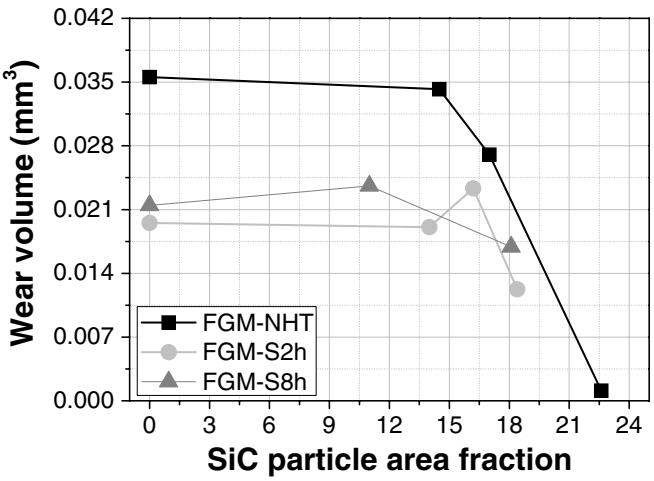

Figure 7. Relation between the wear volume values measured after tribocorrosion tests and the SiC particle area fraction values of FGM-NHT, FGM-S2h and FGM-S8h samples in 0.05M NaCl.

visible SiC particles (figure 8(*b*)) protruding from the surface as shown in the magnified micrograph shown in figures 8(*c*) and (*d*). Between 15% and 18% of SiC particle area fraction, intermediate mechanisms were observed.

Rubbing induced surface transformations in the contacting area of the alumina balls as shown in figure 9. The transformation consisted in crystallographic etching of the

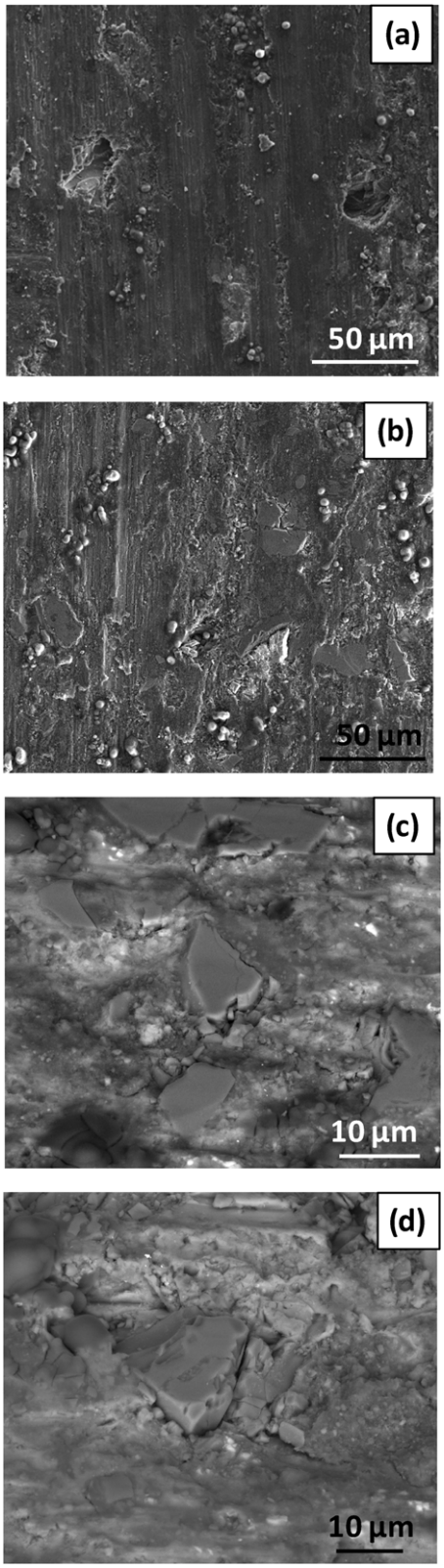

Figure 8. SEM micrographs obtained after the tribocorrosion tests in 0.05M NaCl solution in the wear track of FGM-NHT sample with (*a*) SiC_p particle area fraction of 15 ± 3% obtained in secondary electron mode (SE mode), (*b*) SiC_p particle area fraction of 23 ± 4% (SE mode), (*c*) and (*d*) SiC_p particle area fraction of 23 ± 4% (BE mode, 40° tilted).

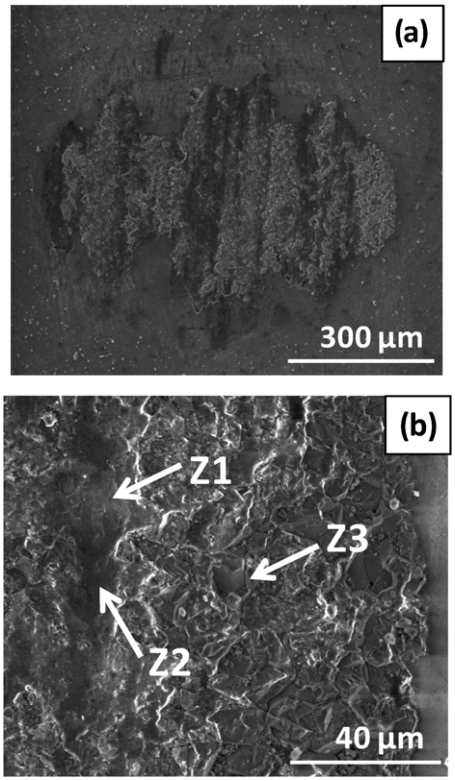

Figure 9. SEM micrographs obtained in the alumina counterbody after the tribocorrosion tests in 0.05M NaCl tested with the FGM-NHT sample (SE mode).

surface and an area of a layer partially covering the ball. This layer was material transferred from the composite counterbody. EDS analysis revealed the presence of Al, Cu, Si and Mg but not of SiC (Z1 and Z2 in figure 9(*b*)). Although the detected Al could be attributed both to the alumina ball and to the Al-matrix alloy, the presence of Si, Cu and Mg strongly suggested the presence of the metallic matrix in the alumina surface. Regarding Z3 zone from figure 9(*b*), only Al and O elements were identified, indicating that, in this zone, only alumina is present.

4. Discussion

Two main mechanisms usually contribute to material degradation in the tribocorrosion of passive metals: wear-accelerated corrosion and mechanical wear [17, 29]. The latter mechanism involves the mechanical removal of metallic particles by counterbody asperities or trapped third body particles digging below the metal surface. Wear-accelerated corrosion arises from the fact that an asperity rubbing on a metal surface produces a track of clean metal which is usually more sensitive to corrosion than the original metal protected by a thin oxide film (passive film). In the present case, the cathodic shift of the potential observed at the onset of rubbing (figure 5) reveals that depassivation and thus wear-accelerated corrosion occur. When rubbing stops the potential recovers its initial (before rubbing) value. For samples with the highest SiC particle area fraction values, the potential recovery occurs already during rubbing indicating that depassivation ceased.

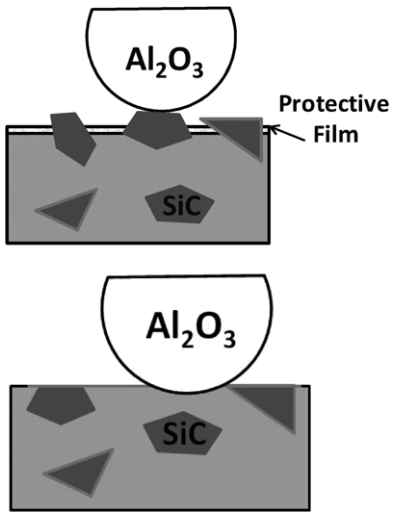

Figure 10. Schematic representation of two wear mechanisms suggested: (*a*) mechanical contact between the protruded SiC reinforcement particles and the Al_2O_3 counterbody; (*b*) mechanical contact between the Al matrix and the Al_2O_3 counterbody.

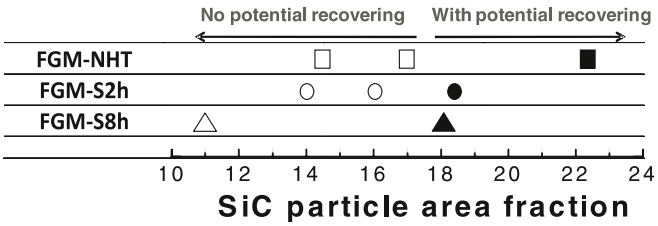

Figure 11. Relation between the potential values measured 100 s before stopping rubbing (at 1700 s) and the SiC particle area fraction values of FGM-NHT, FGM-S2h and FGM-S8h samples tested in 0.05M NaCl. Black symbols represent the situation where potential recover during rubbing was observed.

This particular effect can be explained by the appearance of reinforcement SiC particles standing proud of the aluminium matrix surface (figure 8(*c*)). These protruding SiC particles limit or even suppress direct contact between the metal and the alumina ball as schematically illustrated in figure 10(*a*). In such a situation, depassivation of the aluminium matrix is not expected to occur and thus the wear track recovers the passive state of the surrounding areas and the galvanic coupling effect disappears. For the lowest SiC particle area fraction contents the direct metal/ball contact (figure 10(*b*)) is maintained during the entire rubbing period as indicated by the observed stable cathodic potential shift and the absence on protruding SiC particles. Furthermore, strong wear action on the matrix can lead to pull-out of SiC particles that lose the mechanical support of the surrounding matrix, as shown in figure 8(*a*).

Figure 11 summarizes the observations concerning the passivity recovery during rubbing as a function of heat treatment and SiC content. All samples with a SiC content of 18% or higher exhibit passivity recovery during rubbing. This threshold concentration corresponds well to the SiC content above which protruding reinforcement particles are observed in the wear tracks. It also corresponds to the SiC content above which wear significantly decreases (figure 7).

Clearly, protruding particles not only limits plastic deformation (figure 8) and thus depassivation but they also protect against wear. Interestingly, below 18% the wear intensity is not affected by the presence of SiC reinforcement, the composite materials exhibiting the same wear rate as the unreinforced alloys.

The data obtained here do not permit drawing conclusions about the possible influence of heat treatment on the threshold SiC content for wear transition. More experiments with reinforcement contents around 18% are needed to obtain statistically relevant results. Nevertheless the heat treatment has a clear effect on the overall wear rate. In particular, before the transition, wear is more severe on the non-heat-treated alloy probably due to the lower hardness of the metal matrix.

The two situations depicted in figure 10 may also explain the correlation found between the coefficient of friction and the corrosion potential (figure 6). Indeed, when plastic flow occurs, depassivation is large and thus the potential attains very negative values. This situation corresponds to a direct contact of the alumina counter ball (covered with transferred material) and the composite metal and thus to a specific frictional interaction. When SiC particles protrude from the surface the contact is established between these particles and the counter resulting in a different frictional force and the reduction in plastic deformation of the metal matrix and thus of the cathodic shift of the corrosion potential. The SiC-counter ball contact (figure 10(*a*)) produces less friction than the metal matrix one (figure 10(*b*)). This can be explained by the smooth appearance of the protruding SiC particles and by the suppression of large plastic deformation they induce.

5. Conclusions

The corrosion and tribocorrosion behaviour of Al–SiC_p FGMs in 0.05M NaCl was investigated using samples obtained by centrifugal casting and therefore, presenting different SiC contents in the most exterior part of the tested surfaces. The conclusions of this study are the following:

- The introduction of SiC particles and heat treatments do not affect the corrosion behaviour of the composite materials. The polarization curves follow similar trends with or without reinforcement particles.
- Two tribocorrosion mechanisms observed were depending on SiC_p content: above 18% the SiC particles were found protruding from the surface and thus protecting the surrounding metal matrix against wear and wear-accelerated corrosion. Below 18% the SiC particles had no effect on wear and generalized plastic flow, larger wear and wear-accelerated corrosion characterized the FGMs wearing surfaces.

Acknowledgments

The research team was financially supported by the Portuguese Foundation for Science and Technology (FCT—Portugal) under a PhD scholarship (SFRH/BD/27911/2006). The authors also thank Dr Edith Ariza (University of Minho) and Pierre Mettraux (EPFL) for SEM analysis.

AQ2

References

AQ3

[1] Gasik M M 2003 Industrial applications of FGM solutions *Mater. Sci. Forum* **423** 17–22
[2] Ogawa T, Watanabe Y, Sato H, Kim I and Fukui Y 2006 Theoretical study on fabrication of functionally graded material with density gradient by a centrifugal solid-particle method *Composites* A **37** 2194–200
[3] Duque N B, Melgarejo Z H and Suarez O M 2005 Functionally graded aluminum matrix composites produced by centrifugal casting *Mater. Charact.* **55** 167–71
[4] El-Hadad S, Sato H, Miura-Fujiwara E and Watanabe Y 2010 Fabrication of Al–Al_3Ti/Ti_3Al functionally graded materials under a centrifugal force—review *Materials* **3** 4639–56
[5] Lin D, Li Q, Li W, Zhou S and Swain M V 2009 Design optimization of functionally graded dental implant for bone remodeling *Composites* **40** 668–75
[6] Watari F, Yokoyama A, Omori M, Hirai T, Kondo H, Uo M and Kawasaki T 2004 Biocompatibility of materials and development to functionally graded implant for bio-medical application *Compos. Sci. Technol.* **64** 893–908
[7] Hassanin H and Jiang K 2010 Functionally graded microceramic components *Microelectron. Eng.* **87** 1610–3
[8] Watanabe Y, Kawamoto A and Matsuda K 2002 Particle size distributions in functionally graded materials fabricated by the centrifugal solid-particle method *Compos. Sci. Technol.* **62** 881–8
[9] Watanabe Y, Yamanaka N and Fukui Y 1998 Control of composition gradient in a metal ceramic functionally graded material manufactured by the centrifugal method *Composites* A **29** 595–601
[10] Vieira A C, Sequeira P D, Gomes J R and Rocha L A 2009 Dry sliding wear of Al alloy/SiC_p functionally graded composites: Influence of processing conditions *Wear* **267** 585–92
[11] Velhinho A, Botas J D, Ariza E, Gomes J R and Rocha L A 2004 Tribocorrosion Studies in Centrifugally Cast Al-matrix SiC_p-reinforced functionally Graded Composites *Mater. Sci. Forum* **456** 871–5
[12] Gao J W and Wang C Y 2000 Modeling the solidification of functionally graded materials by centrifugal casting *Mater. Sci. Eng.* A **292** 207–15
[13] Uemura S 2003 The activities of FGM on new applications *Mater. Sci. Forum* **423** 1–10
[14] Mishnaevsky L L Jr 2006 Functionally gradient metal matrix composites: numerical analysis of the microstructure–strength relationships *Compos. Sci. Technol.* **66** 1873–87
[15] Miyamoto Y, Kaysser W A, Rabin B H, Kawasaki A and Ford R G 1999 *Functionally Graded Materials: Design, Processing and Applications* (Kluwer: Academic)
[16] Fang C-K, Huang C C and Chuang T H 1999 Synergistic effects of wear and corrosion for Al_2O_3 particulate–reinforced 6061 aluminium matrix composites *Metall. Mater. Trans.* A **30** 643
[17] Mischler S 2008 Triboelectrochemical techniques and interpretation methods in tribocorrosion: a comparative evaluation *Tribol. Int.* **41** 573–83
[18] Landolt D, Mischler S and Stemp M 2001 Electrochemical methods in tribocorrosion: a critical appraisal *Electrochim. Acta* **46** 3913–29
[19] Montoya-Dávila M, Pech-Canul M I and Pech-Canul M A 2009 Effect of SiC_p multimodal distribution on pitting behaviour of Al/SiC_p composites prepared by reactive infiltration *Powder Technol.* **195** 196–202
[20] Pardo A, Merino M C, Merino S, Viejo F, Carboneras M and Arrabal R 2005 Influence of reinforcement proportion and matrix composition on pitting corrosion behaviour of cast

aluminium matrix composites (A3xx.x/SiC_p) *Corros. Sci.* **47** 1750–64

[21] Gomes J R, Ribeiro A R, Vieira A C, Miranda A S and Rocha L A 2005 Wear mechanisms in functionally graded aluminium matrix composites: effect of the presence of an aqueous solution *Mater. Sci. Forum* **493** 33–8

[22] Vieira A C, Rocha L A and Mischler S 2010 Mechanical and electrochemical deterioration mechanisms in the tribocorrosion of Al alloys in NaCl and in $NaNO_3$ solutions *Corrosion Sci.* submitted

[23] Stojadinovic J, Bouvet D, Declercq M and Mischler S 2009 Effect of electrode potential on the tribocorrosion of tungsten *Tribol. Int.* **42** 575–58

[24] Vieira A C, Pinto A M, Rocha L A and Mischler S 2011 Effect of Al_2Cu precipitates size and mass transport on the polarization behavior of age-hardened Al–Si–Cu–Mg alloys in 0.05M NaCl *Electrochim. Acta* doi:10.1016/j.electacta.2011.02.044

[25] Mondal D P and Das S 2006 High stress abrasive wear behavior of aluminum hard particle composites: Effect of experimental parameters, particle size and volume fraction *Tribol. Int.* **39** 470–8

[26] Ponthiaux P, Wenger F, Drees D and Celis J P 2004 Electrochemical techniques for studying tribocorrosion processes *Wear* **256** 459–68

[27] Taylor D E and Waterhouse R B 1974 An electrochemical investigation on fretting corrosion of a number of pure metals in 0.5M sodium chloride *Corros. Sci.* **14** 111–22

[28] Bethune B and Waterhouse R B 1968 Electrochemical studies of fretting corrosion *Wear* **12** 27–34

[29] Landolt D 2007 *Corrosion and Surfaces Chemistry of Metals* 1st edn (EPFL Press)

QUERIES

Page 1
AQ1
Please be aware that the colour figures in this article will only appear in colour in the web version. If you require colour in the printed journal and have not previously arranged it, please contact the Production Editor now.

Page 8
AQ2
Please note that superscript ‘a’ (after Dr) has been deleted in the acknowledgement section. Please confirm the change.

Page 8
AQ3
Please check the details for any journal references that do not have a blue link as they may contain some incorrect information. Pale purple links are used for references to arXiv e-prints.

Page 9
AQ4
Please provide volume and page range for refs. [22,24].

Page 9
AQ5
Please provide place of publisher for ref[29].